Human Molecular Genetics, 2012, Vol. 21, No. 6 **1248–1259**
doi:10.1093/hmg/ddr555
Advance Access published on November 24, 2011

GLUT10 is required for the development of the cardiovascular system and the notochord and connects mitochondrial function to TGFβ signaling

Andy Willaert[1,3,†], Sandeep Khatri[4,†], Bert L. Callewaert[1,3], Paul J. Coucke[3], Seth D. Crosby[2], Joseph G. H. Lee[8], Elaine C. Davis[8], Sruti Shiva[5,6], Michael Tsang[7], Anne De Paepe[3] and Zsolt Urban[1,2,4,*]

[1]Department of Pediatrics and [2]Department of Genetics, Washington University School of Medicine, St. Louis, MO, USA, [3]Department of Medical Genetics, Ghent University Hospital, Ghent, Belgium, [4]Department of Human Genetics, Graduate School of Public Health, [5]Vascular Medicine Institute, Department of Medicine, [6]Department of Pharmacology and Chemical Biology and [7]Department of Developmental Biology, University of Pittsburgh, PA, USA and [8]Department of Anatomy and Cell Biology, McGill University, Montreal, Canada H3A 2B2

Received October 31, 2011; Revised October 31, 2011; Accepted November 21, 2011

Growth factor signaling results in dramatic phenotypic changes in cells, which require commensurate alterations in cellular metabolism. Mutations in *SLC2A10*/GLUT10, a member of the facilitative glucose transporter family, are associated with altered transforming growth factor-β (TGFβ) signaling in patients with arterial tortuosity syndrome (ATS). The objective of this work was to test whether *SLC2A10*/GLUT10 can serve as a link between TGFβ-related transcriptional regulation and metabolism during development. In zebrafish embryos, knockdown of *slc2a10* using antisense morpholino oligonucleotide injection caused a wavy notochord and cardiovascular abnormalities with a reduced heart rate and blood flow, which was coupled with an incomplete and irregular vascular patterning. This was phenocopied by treatment with a small-molecule inhibitor of TGFβ receptor (tgfbr1/alk5). Array hybridization showed that the changes at the transcriptome level caused by the two treatments were highly correlated, revealing that a reduced tgfbr1 signaling is a key feature of ATS in early zebrafish development. Interestingly, a large proportion of the genes, which were specifically dysregulated after glut10 depletion gene and not by tgfbr1 inhibition, play a major role in mitochondrial function. Consistent with these results, *slc2a10* morphants showed decreased respiration and reduced TGFβ reporter gene activity. Finally, co-injection of antisense morpholinos targeting *slc2a10* and *smad7* (a TGFβ inhibitor) resulted in a partial rescue of *smad7* morphant phenotypes, suggesting *scl2a10*/glut10 functions downstream of smads. Taken together, glut10 is essential for cardiovascular development by facilitating both mitochondrial respiration and TGFβ signaling.

INTRODUCTION

Growth factor signaling requires a close coupling to metabolism to direct growth and development and to maintain homestasis. For example, the phosphoinositide 3-kinase/protein kinase B/mammalian target of rapamycin (PI3K/AKT/mTOR) pathway integrates proliferative insulin-like growth factor signals, the availability of amino acids, cellular energy and oxidative potential with protein synthesis (1). TGFβ growth factors provide essential signals in cardiac and vascular development (2) and are key initiators of the fibrotic response in a variety of disease states including myocardial infarction (3) and atherosclerosis (4). Typically, TGFβ signals elicit reduced cell proliferation, epithelial–mesenchymal transition, assumption of migratory phenotypes, elevated synthesis of

*To whom correspondence should be addressed at: Department of Human Genetics, Graduate School of Public Health, University of Pittsburgh, 130 DeSoto Street, Crabtree Hall A300, Pittsburgh, PA 15261, USA. Tel: +1 4126488269; Fax: +1 4126243020; Email: urbanz@pitt.edu
†The authors wish it to be known that, in their opinion, the first 2 authors should be regarded as joint First Authors.

both structural and remodeling components of the extracellular matrix (ECM) and elaboration of a contractile cytoskeleton. We postulate that such dramatic phenotypic changes require metabolic integration.

As a way to define shared molecules in the TGFβ signaling and metabolic pathways, we focused on *SLC2A10*/GLUT10, a member of the facilitative glucose transporter family. Mutations in *SLC2A10* cause arterial tortuosity syndrome (ATS—OMIM#208050), a recessively inherited disorder characterized by elongation, tortuosity, stenosis and aneurysms of the large and medium sized arteries in association with distinct craniofacial and connective tissue manifestations (5,6). Functional analysis of patient tissue samples has shown that a loss of function of GLUT10 may lead to vascular malformations via upregulation of the TGFβ signaling pathway in the arterial wall.

Increased TGFβ signaling in association with arterial aneurysm formation (and tortuosity) is a common finding in aortic aneurysm syndromes such as Marfan syndrome, caused by heterozygous mutations in the *FBN1* gene (7), Loeys–Dietz syndrome caused by heterozygous mutations in the genes encoding the TGFβ receptors 1 and 2 (*TGFBR1* and *TGFBR2*) (8) and autosomal-recessive cutis laxa due to fibulin 4 deficiency (9,10). Involvement of TGFβ upregulation in the pathogenesis of Marfan syndrome has been illustrated in a mouse model in which several clinical features, including pulmonary emphysema, aortic root dilatation and skeletal muscle dysfunction, could be prevented and reversed after administration of TGFβ neutralizing antibodies or a pharmacological inhibitor of the pathway, losartan (7,11,12). Despite the association of TGFβ upregulation with ATS, the developmental origin of vascular malformations in these diseases remains unclear, and in some cases, conflicting. For example, the reported elevation of TGFβ signaling in Loeys–Dietz syndrome blood vessels is paradoxical because these patients carry inactivating mutations in either *TGFBR1* or *TGFBR2* (8).

The exact role of GLUT10 in the TGFβ signaling pathways and metabolism remains to be elucidated. Mice with homozygous missense substitutions in GLUT10 do not show the same severe vascular abnormalities as encountered in human ATS patients and therefore these models are of limited use to investigate the pathogenetic mechanisms underlying human ATS (13,14). Because recent studies suggest that the zebrafish is a very useful organism to study cardiovascular disorders (15), we aimed to establish an ATS zebrafish model by knocking down the zebrafish *slc2a10* gene. Using small molecule treatment and gene expression profiling experiments, we show a significant overlap between glut10 function and the TGFβ signaling pathway. Moreover, we find that expression of several genes necessary for cellular respiration are altered by glut10 deficiency. Finally, functional assays indicate that glut10 is required both for mitochondrial respiration and for optimal TGFβ signaling.

RESULTS

Zebrafish *slc2a10*/glut10 structure

The zebrafish *slc2a10* gene is located on chromosome 11. The gene structure is similar to the human homologue and also contains five exons of similar size, although intronic sequences and untranslated regions are shorter (Fig. 1A). The structure of human GLUT10, the protein encoded by *SLC2A10*, contains 12 hydrophobic transmembrane domains (TMD) with two large hydrophilic exofacial and endofacial loops. Hydropathy analysis reveals an identical structure for zebrafish glut10 (Supplementary Material, Fig. S1). Aligning the amino acid sequence of human and zebrafish GLUT10 shows a homology of 43%, with the major structural differences being a shorter and divergent exofacial loop 9 between TMD 9 and 10 and a divergent endofacial loop 6 between TMD 6 and 7 in glut10 (Fig. 1B). The N^{334}ATG glycosylation motif in the large exofacial loop 9 in GLUT10, which is a hallmark of the class 3 sugar transport facilitators, is replaced by an N^{341}LTL glycosylation motif in the same loop in glut10 (PROSITE analysis). Similar to its human homologue, glut10 retains most of the sugar transporter signatures, which are characteristic of the mammalian glucose transporters in general and of the subfamily of class 3 sugar transport facilitators in particular.

Slc2a10 knockdown phenotype

Slc2a10 is provided to the embryo as a maternal transcript and is widely expressed during gastrulation, segmentation and pharyngula periods, suggesting a developmental role for this transporter (16). To reveal the role of the *slc2a10* gene in zebrafish development, we performed knockdown experiments with two different antisense morpholino oligonucleotides (MOs). One MO was targeting the *slc2a10* start codon (ATG-MO) and is complementary to parts of exons 1 and 2 (Fig. 1A). The second MO was a splice-blocking MO, complementary to the exon 2–intron 2 donor splice site (splice-MO). Injection of 2.5 ng of ATG-MO caused phenotypic abnormalities, showing a relatively broad range of severity in gross morphology. With increasing severity, one could distinguish wild-type embryos, class 1 embryos characterized by a bowed notochord/tail, class 2 embryos with a wavy notochord or tail and class 3 embryos which were very small and showed extensive tissue dysplasia especially in the tail region (Fig. 2A and Table 1).

Injection of 7.5 ng of splice-MO caused identical phenotypes with almost identical frequencies for the different classes. Injection of a scrambled control-MO, which has no target in the zebrafish genome, did not cause any visible phenotypic abnormalities compared with uninjected embryos. Survival curves also indicated similar, 5–10% reduction of survival in both ATG- and splice-MO-injected embryos compared with control-MO-injected embryos at 120 hours post-fertilization (hpf; Supplementary Material, Fig. S2). This was due to the high mortality of severely affected class 3 embryos which comprised ∼10% of the ATG- and splice-MO-injected embryos.

Next, we investigated the effect of the splice-MO on *slc2a10* mRNA splicing by performing reverse transcription polymerase chain reaction (RT–PCR) with primers in exons 1 and 3 of the *slc2a10* gene. As expected, we found that injection of the splice-MO resulted in the skipping of exon 2 (Fig. 3), which caused a frameshift and a premature termination codon. The resulting transcript was 50% less abundant than *slc2a10* mRNA in control embryos, presumably as a consequence of nonsense-mediated decay.

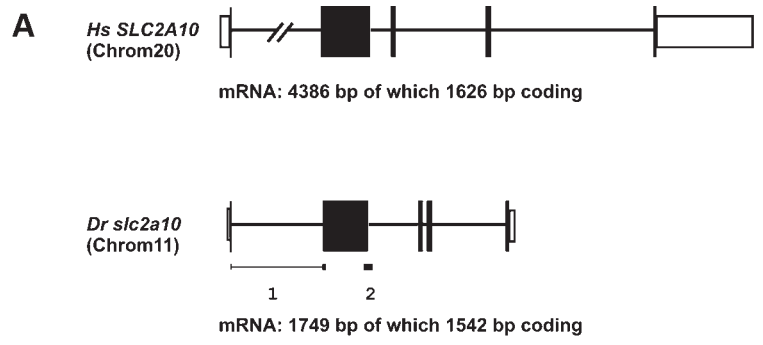

B

```
                                TMD1                                                TMD2                                                TMD3
NP_110404.1[Hs]     MGHSPPVLPLCASVSLLGGLTFGYELAVISGALLPLQLDFGLSCLEQEFLVGSLLLGALLASLVGGFLIDCYGRKQAILGSNLVLLAGSLTLGLAGSLAW 100
XP_594277.3[Bt]     MGRPSLLLPLCASVSLLGGLTFGYELAVISGALLPLQLDFGLSCSQQELLVGSLLLGALLASLVGGCLIDRYGRKQAILGSNLVLLAGSLSLGLAGSLAW 100
NP_569718.1[Mm]     MGLRPAVLLLCASVSLLGGLTFGYELAVISGALLPLQLNFGLSCLEQELLVGSLLLGALLASLVGGFLIDCYGRRRAILGSNAVLLAGSLILGLASSLPW 100
NP_001102433.1[Rn]  MGLGPTVLPLCASVSLLGGLTFGYELAVISGALLPLQLDFRLSCLEQELLVGSLLLGAFLASLVGGFLIDCYGRRRAILGSNVVLLAGSLILGLAGSLPW 100
XP_417383.2[Gg]     MGRALLVLLLSAAVSLLGGLIFGYELGIISGALLQLQADFSLGCFKQEVLVSSLLVGAFLASLVGGILIDRHGRRRAILVSNVVLLFGSLILTLTRSFTG 100
NP_001072926.1[Xt]  MGLSSPTLILAATVSLLGGIVFGYELGIISGALLVLKTVYQLTCFEQEALVSAVLFGALLASLIGGIIIDRWGRRTAILASNLVVLAGSIILIATSTFWV 100
NP_001104633.1[Dr]  MGCS--VLLLTITVSTLGGLVFGYELGIISGALPQLQTHFSLGCVQQEAVVSALLIGSLFASIIGGWLIDRHGRRTSILLSNLLILTGSVILTTGTSFFA 98
                    **     * *  :** ***: ****** .:***** *:  : * * :** :*.::*.*::::**::** :**  **:  :** ** ::* **: *    ::

                                TMD4                                                TMD5                                                TMD6
NP_110404.1[Hs]     LVLGRAVVGFAISLSSMACCIYVSELVGPRQRGVLVSLYEAGITVGILLSYALNYALAGTPWG-WRHMFGWATAPAVLQSLSLLFLPAG-----TDETAT 194
XP_594277.3[Bt]     LLLGRSVAGFAISLSSMACCIHVSELAGPRQRGVLVALYEAGITVGVLLSYALNYALAGAPRG-WRHMFGWAAAPALLQSLSLLFLPAG-----TVRAAA 194
NP_569718.1[Mm]     LLLGRLSVGFAISLSSMACCIYVSELVGPRQRGVLVSLYEVGITVGILFSYGLNYVLAGSPWG-WRHMFGWAAAPALLQSLSLFLLPAG-----AEGTAA 194
NP_001102433.1[Rn]  LLLGRSSVGFAISLSSMACCIYVSELVGPRQRGVLVSLYEVGITVGILFSYGLNYVLAGSPWG-WRHMFGWAAAPALLQSLSLFFLPAG-----AEGTAA 194
XP_417383.2[Gg]     LVLGRMAVGFAISVSSMGCCIYVSEMVAAHQRGLLVSLYEAGITVGILLSYALNYAFADTREG-WRYMFGLAMAPAAMQFLSILFLPVNPVKLNTWDSDC 199
NP_001072926.1[Xt]  LIVGRVTIGFAISISSMACCIYVSEIVRPHQRGMLVSLYETGITVGILISYAMNYFLSGVNES-WKYMFGLAIVPAAFQFISILFLPSKPHKLNFWEQDT 199
NP_001104633.1[Dr]  LVIGRAVIGFAMTVSSMSCCIFVSEMVTPERRGLMVTLYEVGVTVGILIAYAVNYFFNNVQLTGWRYMFGFAIIPSLIQLASIVLLPKQAEVFVIHDDDS 198
                    *::**   ***:::***.***.***:. ..:**::*:***.*:***:*::*.:** : .    *:*:*** *  *: :*  *:.:**

                                                                                    TMD7                                                TMD8
NP_110404.1[Hs]     HKDLIPLQGGE---APKLGPGRPR-YSFLDLFRARDNMRGRTTVGLGLVLFQQLTGQPNVLCYASTIFSSVGFHGGSSAVLASVGLGAVKVAATLTAMGL 290
XP_594277.3[Bt]     LKDLIPLQGGE---ATKLDPGRPR-YAFVDLFRARDNMRVRTVVGLGLVLFQQLTGQPNVLAYASTIFQSVGFQGGSSAVLASVGLGAVKVAATLMAMGL 290
NP_569718.1[Mm]     PKDLIPLQGRE---TSKPGLVKPQ-YSFLDLFRAQDGMWSRTVVGLGLVLFQQLTGQPNVLYYASTIFRSVGFHGGSSAVLASVGLGTVKVAATLVATGL 290
NP_001102433.1[Rn]  RQDLIPLQGGE---TSKLGLVKAQ-YTFLDLFRAQDGMWSRTVVGLGLVLFQQLTGQPNVLYYASTIFRSVGFHGGSSAVLASVGLGTVKVVATLIATGL 290
XP_417383.2[Gg]     QKGLIQLQTAEDREAAKREPYKEKHYSFLDLFRTRDNMRRRTLVGLGLVLFQQFTGQPNVLGYASKIFHSVGFQSNSSAILASVGLGAIKVVATLVAMAF 299
NP_001072926.1[Xt]  DDGFIELEETGEAGEFKPDTYDRQ-YTFLDLFRSKDNMRTRTLLGLGLVLFQQFTGQPNVLYYASTIFQSVGFQSNSSAVLASVGLGVVKVASTLIAICF 298
NP_001104633.1[Dr]  RQADRLTEETE---TSNQHQQSEK-YGVSDLFKSKDNMRRRTVIGVGLVLSQQFTGQPNVLFYASTILFSVGFQSNASAILASVGFGIVKVIATLLAMLC 294
                     .     :       :      : * . ***:::*.*  ** :*:**** **:******* ***.*: ****:..:**:*****:* :** :** *

                                TMD9
NP_110404.1[Hs]     VDRAGRRALLLAGCALMALSVSGIGLVSFAVPMDSGPSCLAV-PNATGQTGLPGDSGLL--QDSSLPPIPRTNE--------------------DQREPIL 368
XP_594277.3[Bt]     VDRAGRRALLLAGCALMALSVSGLGLVSFAVPLHSGPACLAV-PNATRLSGFPGDSGLP--RGLAPPLPPTTDQ--------------------SPRQPVL 368
NP_569718.1[Mm]     VDRAGRRVLLLFGCALMALSVSGIGLVSFAVSLDSGPSCLAT-SNASQQVDLPGSSGLL--VRSSLPPVLHTNG--------------------DQGQLVL 368
NP_001102433.1[Rn]  VDRVGRRALLLSGCALMALSVSGIGLVSFAVSLDSGPSCLAT-SNTSQQVDLPQTPGLL--VRTSLPPVLHTSG--------------------DQGQPVR 368
XP_417383.2[Gg]     ADKAGRRALLLAGAVVMAISVTTIGLSSCIAPLAMARDCTAA-ADPNVSHSLPQHPLAP--PSSHIPPDLGEGNGWAGPGSAATKSLTKALASARGSEVV 396
NP_001072926.1[Xt]  ADKAGRRILLLAGCIVMTIAITGIGIVSFTVKMDSHRDCGSV-TGRNMSSGESNVSQLLGIVHAETSTINTLDN--------------------SVHQLAM 378
NP_001104633.1[Dr]  SDRAGRRSLLIGGCSMLAVGLILTGFLCTQSVIDTTKRCTSVGPHSNLTLSAEHEEGVG----------------------------------FSSQTL 359
                    *:.*** **: *. :::::.:   *: .    :     * :. .  .   .                                          .

                                                                                    TMD10                                               TMD11
NP_110404.1[Hs]     STAKKTKPHPRSGDPSAPPRLALSSALPGPPLPARGHALLRWTALLCLMVFVSAFSFGFGPVTWLVLSEIYPVEIRGRAFAFCNSFNWAANLFISLSFLD 468
XP_594277.3[Bt]     STSEKTRPPPGAEDP-----TALSLTPPARLSPTPEHALLHWTALVCMMVFVSAFSIGFGPVTWLVLSEIYPVEIRGRAFAFCNSFNWAANLFISLSFLD 463
NP_569718.1[Mm]     SVTERPIHPVITASLG----PVLNTASPVPTSPILEHTLLCWSALVCMMVYVSAFSVGFGPVTWLVLSEIYPAEIRGRAFAFCSSFNWAANLFISLSFLD 464
NP_001102433.1[Rn]  SVTERPIHPVITASLG----PALNIDSSVPTSPIPEHTLLCWSALVCMMVYVSAFSFGFGPVTWLVLSEIYPVEIRGRAFAFCSSFNWAANLFISLSFLD 464
XP_417383.2[Gg]     TRSSHTRKVGLVGQPEK--ETAESTEPPFGSAPLTEHMVLNWITLLSMMAFVSAFSIGFGPMTWLVLSEIYPAGIRGRAFAFCNSFNWAANLLISLSFLD 494
NP_001072926.1[Xt]  AIRSPSLANSASSNHKD-LISQNSTVLPASPELPSNYTILNWITLLSMMAFVSAFSIGFGPMTWIVLSEIYPADIRGRAFAFCNSFNWAANLLITLTFLD 477
NP_001104633.1[Dr]  DVHEHLRSFS-----------------------QSEDIYKWIIFTCLMAVVSAFSVSFGPMTWVVLSEIFPKDIRGRAFSFINCFNVGTNLIVTFSFLS 435
                       .                             :  *  : .:*. *****..*:**:**:****:*  ******:* ..** .:**::::**.

                                TMD12
NP_110404.1[Hs]     LIGTIGLSWTFLLYGLTAVLGLGFIYLFVPETKGQSLAEIDQQFQKRRFTL------SFGHRQNS------TGIPYSRIEISAAS- 541
XP_594277.3[Bt]     LIGAIGLSWTFLLYGLTAVFGLGFIYLFVPETKGQSLADIDQQFQKKWFPL------SFGHRQSS------AGVQYSRIEVSAAS- 536
NP_569718.1[Mm]     LIGAIGLAWTFLLYGLTAVLGLAFIYLLVPETKGQSLAEIEQQFQTSRFPL------NFGHRQR-------IGIQYHRLDVSSAS- 536
NP_001102433.1[Rn]  LIGAIGLAWTFLLYGLTAVLGLAFIYLLVPETKGQSLAEIEQQFQMRRFPL------SFGHRQH-------SGIQYRRLEVSSAS- 536
XP_417383.2[Gg]     LIDAIGFSWMFLLYGLMGVMAVIFIYFFVPETKGQSLEEIDQQFSRKWLRE------GSGCKQRRARGASCAHGQYQRVERASSA- 573
NP_001072926.1[Xt]  VIASIGLSWTFLLYGVVGLLAIAFIYFFIPETKGQSLEEIDKQFSTKRILQKRETSKGVGKRPS-------SGPPYQRIGKASPS- 555
NP_001104633.1[Dr]  IIDVIGLSGVFLMYGVVGIAGVVFIYLVLPETKGKSLQDIDRELSQTRMIHR-QELCSIFQRRR-------FSPGYQRVQLTSTAT 513
                    :*  **::  **:**: .: .: ***:.:*****:** :*::::.   :        .   :            * *:  ::.:
```

Figure 1. Evolutionary conservation of the *SLC2A10* gene and GLUT10 protein. (**A**) The structure of the human *SLC2A10* and the zebrafish *slc2a10* genes with coding (full boxes) and untranslated (empty boxes) regions shown. MO target regions 1 and 2 are depicted underneath the *slc2a10* gene structure. (**B**) Multiple amino acid sequence alignment of GLUT10 among different species (Clustal W2) (46). Predicted TMDs for human GLUT10 are marked by black bars (47). Boxes indicate sequence motifs, conserved in vertebrate glucose transporters or class 3 sugar transporter facilitators, which are also conserved for GLUT10 among different species including zebrafish (47,48). The N^{341}LTL glycosylation motif in glut10 is underlined. Conservation of amino acid sequences are shown below the alignment: '*' means residues identical in all sequences in the alignment; ':' means conserved substitutions; '.' means semi-conserved substitutions; space means no conservation. *Hs*, human; *Bt*, cow; *Mm*, mouse; *Rn*, rat; *Gg*, chicken; *Xt*, frog; *Dr*, zebrafish.

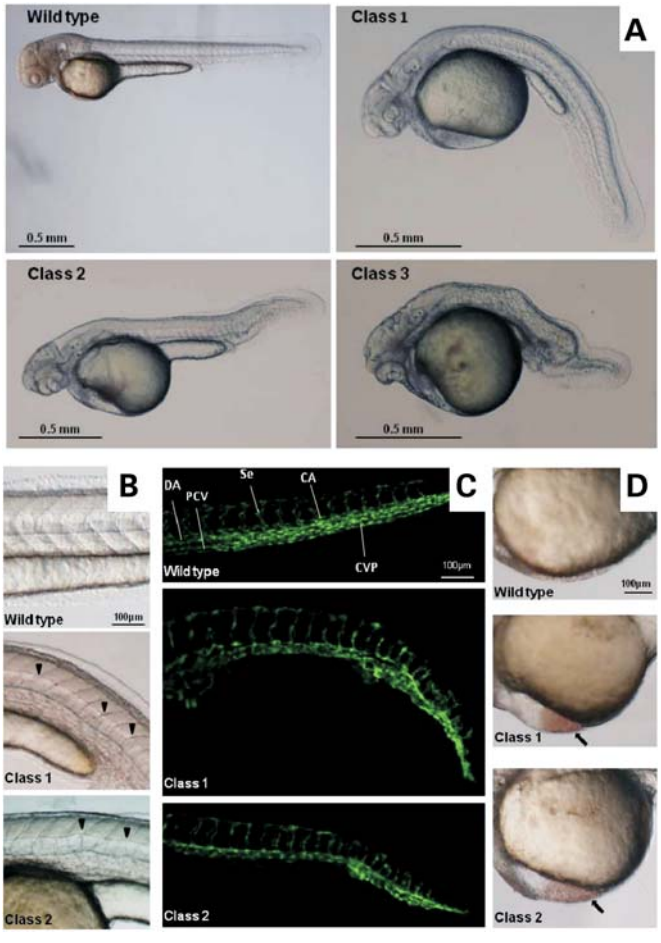

Figure 2. *Slc2a10* knockdown phenotype. (**A**) General morphology of *slc2a10* morphants at 48 hpf. Besides wild-type embryos, three different embryo classes can be discerned based on general notochord/tail structure. (**B**) Class 1 and 2 morphants exhibit bowing and kinking of the notochord (arrowheads). (**C**) Confocal microscopy in *Fli1:eGFP* zebrafish injected with *slc2a10* splice-MO. In Class 1 and 2 embryos, the vasculature is incomplete and shows irregular patterning, especially of the caudal vein plexus. (**D**) Blood pooling in the sinus venosus of the heart (black arrows). DA, dorsal aorta; Se, segmental vessels; CA, caudal artery; CVP, caudal vein plexus.

Table 1. Phenotype classification of slc2a10-MO-injected embryos at 48 hpf

Morpholino	Morpholino dose (ng)	Wild type (%)	Class 1 (%)	Class 2 (%)	Class 3 (%)	*n*
Uninjected	0	95.8	0.8	3.4	0.0	118
control-MO	5	97.4	0.0	2.6	0.0	114
ATG-MO	2.5	24.1	38.9	25.9	11.1	54
splice-MO	7.5	23.5	39.0	28.7	8.8	136

Class 1: embryos with a bowed notochord/tail; Class 2: embryos with wavy notochord or tail; Class 3: very small embryos and extensive tissue malformation especially in the tail region. Results for every MO were obtained from at least three independent injections. χ^2 or Fisher's exact tests revealed no significantly different distribution of classes ($P > 0.05$) between uninjected and control-MO and between ATG-MO and splice-MO while significant differences ($P < 0.001$) could be detected between uninjected or control-MO versus ATG-MO or splice-MO.

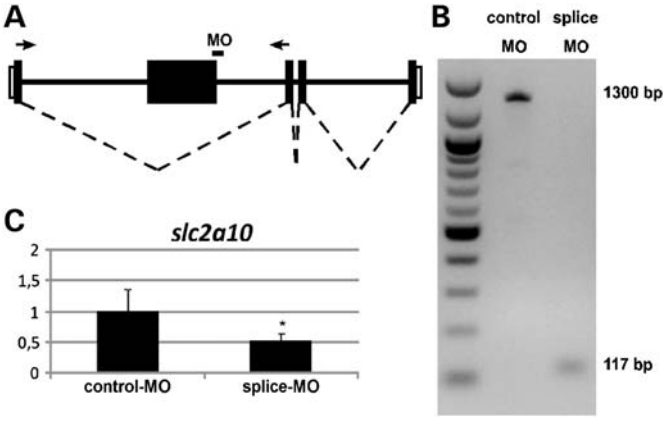

Figure 3. MO knockdown of *slc2a10*. (**A**) Schematic representation of *slc2a10* splicing after splice-MO injection. A black bar represents the target position of the splice-MO. Arrows denote the position of the RT–PCR primers in exons 1 and 3. (**B**) Agarose gel electrophoresis of *slc2a10* RT–PCR samples (from control- and splice-MO-injected embryos). In control-MO-injected embryos, a 1300 bp product corresponds to the full-length *slc2a10* mRNA. In splice-MO-injected embryos, a 117 bp fragment represents skipping of exon 2. (**C**) Quantitative PCR analysis shows a 50% reduction in *slc2a10* expression in splice-MO-injected compared with control-MO-injected embryos. $^*P < 0.05$ (95% confidence intervals of the means do not overlap).

We were not able to check whether the ATG-MO effectively inhibited translation as no antibodies that target the glut10 protein were available. Therefore, we performed the subsequent experiments using the splice-MO instead of the ATG-MO. We also focused on 48 hpf embryos. At this stage, most of the internal organs are developed including a fully functional cardiovascular system (17). Moreover, at 48 hpf, diffusion-mediated gas exchange still suffices for basic metabolic supplies in the embryos, which makes them independent of convective blood circulation, avoiding secondary effects of circulatory abnormalities.

The 48 hpf morphants were significantly smaller with a reduced embryo/yolk sac extension length ratio (Table 2). They had a bowed (class 1) or wavy (class 2) tail with notochord abnormalities (Fig. 2B). Cardiac edema was frequently observed and most of the embryos showed cardiovascular abnormalities with a reduced heart rate and blood flow, incomplete and irregular patterning of the vasculature especially in the tail, eventually causing blood pooling in the sinus venosus of the heart and in the tail region (Fig. 2C and D).

Inhibition of TGFβ pathway in zebrafish by drug administration

Because abnormal TGFβ signaling has been shown in cells and tissues from human ATS patients, we performed pharmacological studies to evaluate the effect of the *slc2a10* knockdown on the TGFβ pathway. We used a TGFβ type 1 receptor kinase inhibitor (ALK5 inhibitor, LY-364947), which specifically targets the TGFBR1 kinase function and which is, in contrast to other TGFBR1 inhibitors, much less potent against related kinases such as TGFBR2 (18,19). Blocking this kinase inhibits phosphorylation of SMAD2 and SMAD3 and downregulates the TGFβ signaling. Alignment of the amino acid sequence of human TGFBR1 with

Table 2. Impaired growth and circulation in slc2a10 splice-MO-injected embryos compared with control-MO-injected embryos at 48 hpf

	Control-MO	Splice-MO Wild type	Class 1	Class 2
Embryo length (mm)[a]	2.95 ± 0.21	2.73 ± 0.22***	2.11 ± 0.30***	2.15 ± 0.43***
Yolk sac extension length (mm)[a]	0.76 ± 0.07	0.63 ± 0.09***	0.44 ± 0.08***	0.44 ± 0.15***
Yolk sac extension/embryo length ratio	0.26 ± 0.02	0.23 ± 0.02***	0.21 ± 0.02***	0.20 ± 0.04***
Heart rate (bpm)	125.46 ± 9.91	113.25 ± 17.43**	101.31 ± 17.67***	95.50 ± 15.93***
Abnormal blood flow	12/114	2/32	13/52*	23/40***
Blood pooling	14/114	2/32	12/52	18/40***

For continuous variables including embryo length, yolk sac extension length, yolk sac extension length/embryo length ratio and heart rate, statistical analysis was conducted using non-parametric Kruskal–Wallis followed by Dunn's multiple comparison post hoc tests. For categorical variables including blood flow and blood pooling a χ^2 test was followed by Bonferroni correction. Standard deviations from the mean are indicated for continuous variables (± SD).
[a]Longest linear dimension.
*$P < 0.05$.
**$P < 0.01$.
***$P < 0.001$.

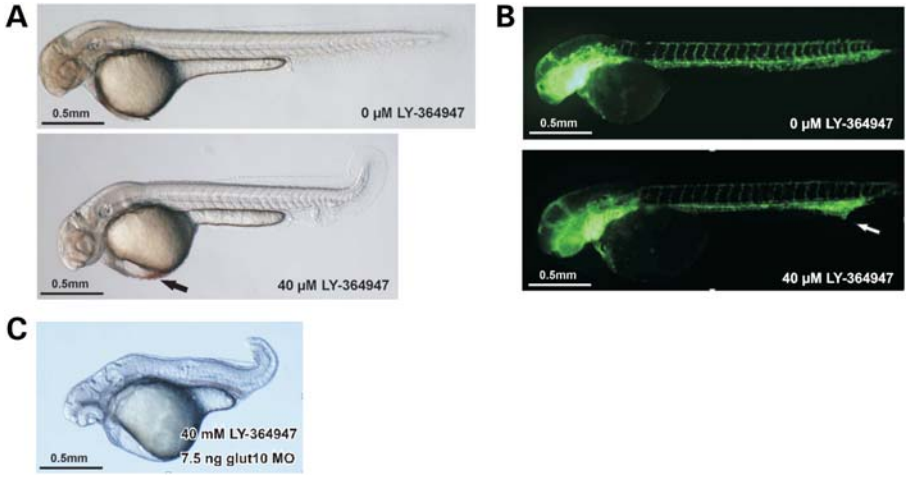

Figure 4. Tgfbr1 inhibitor (LY-364947) treatment. (**A**) Wild-type fish treated with 0 and 40 µM LY-364947. Blood pooling in the sinus venosus is indicated by a black arrow. (**B**) *Fli1:eGFP* fish treated with 0 or 40 µM LY-364947. Condensation of the caudal vein plexus is marked by a white arrow. (**C**) Splice-MO-injected embryo treated with 40 µM LY-364947.

both zebrafish tgfbr1a and tgfbr1b revealed a high level of conservation (77 and 79%, respectively, data not shown) with almost complete conservation of the kinase domain (96%). This provided a strong structural basis for the use of LY-364947 on zebrafish embryos.

We applied an LY-364947 dilution series ranging from 0 to 100 µM to wild-type embryos to assess toxic effects or to detect specific phenotypes (Supplementary Material, Table S1). At 10 µM no abnormalities were observed, whereas at ≥80 µM all embryos died. At a concentration of 40 µM, a specific dysmorphic phenotype could be detected in almost all embryos (Fig. 4A). The observed anomalies were similar to those found in *slc2a10* knockdown embryos (compare Fig. 4A, LY-treated embryo, with Fig. 2A, class I embryo). The embryos were significantly smaller, showed bowing of the tail and notochord, low heart rate, vascular abnormalities, no blood flow with blood pooling in the sinus venosus. In *Fli1:eGFP* fish, treated with 40 µM LY-364947, condensation of the caudal vein plexus, a structure that slowly remodels into a single vascular tube during embryogenesis, was observed (Fig. 4B). Inhibition of TGFβ signaling did not influence the expression of the *slc2a10* gene assayed by quantitative RT–PCR (qPCR), indicating that *slc2a10* was not subject to feedback regulation by the TGFβ pathway (data not shown). Finally, treatment of splice-MO-injected embryos with 40 µM LY-364947 made the phenotype even more severe, yielding embryos that all belonged to the severe class 3 (Fig. 4C).

Transcriptome analysis in *slc2a10* knockdown and LY-364947 treated zebrafish

To further elucidate the role of GLUT10 function in the TGFβ and other signaling pathways, we looked for similarities and differences in the global zebrafish transcript profiles caused by reduced *slc2a10* expression and by tgfbr1 inhibition. We extracted RNA from 48 hpf embryos and prepared cDNA with a two-color-labeling procedure, which was subsequently loaded on Agilent expression arrays consisting of 43 803 60mer probes. First, we compared gene expression in embryos injected with *slc2a10* splice-MO versus control-MO. Secondly, we compared gene expression in embryos treated

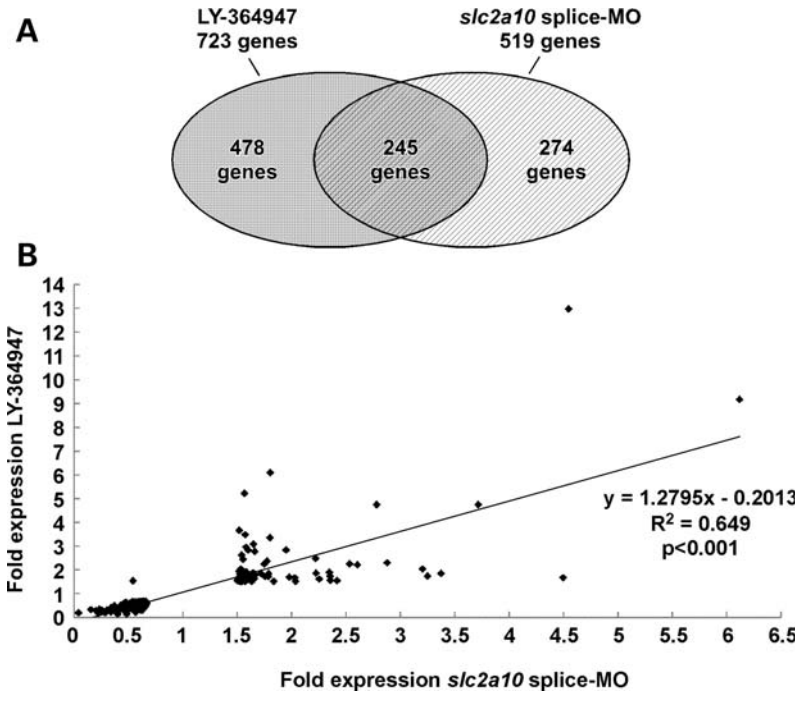

Figure 5. Transcriptome analysis in *slc2a10* knockdown and tgfbr1 (LY-364947) inhibitor-treated zebrafish. (**A**) Venn diagram depicting the overlap between differentially expressed gene transcripts ($\geq$1.5-fold expression; $P < 0.05$) after LY-364947 treatment and after splice-MO injection. (**B**) The correlation between gene transcripts with transcript-level changes of $\geq$1.5-fold ($P < 0.05$) after splice-MO injection and after LY-364947 treatment (Pearson correlation).

with LY-364947 versus untreated embryos. To establish gene sets that were overexpressed or underexpressed, we took as a cut-off transcript-level changes of $\geq$1.5-fold relative to the control samples. We compared the differentially expressed gene sets between both experiments to define specific gene subsets that are common. Of the 519 genes that were over- or underexpressed in the *slc2a10* knockdown model, ~50% (245 genes) were also dysregulated by LY-364947 (Fig. 5A). Furthermore, most of the genes that were dysregulated by both treatments were up- or downregulated in the same direction and to the same extent, as indicated by the strong correlation ($r = 0.81$) between their mean expression ratios (Fig. 5B). Consistent with known functions of TGFβ, many genes important for cardiovascular, cartilage and eye development and neurogenesis were downregulated (Supplementary Material, Table S2). In contrast, genes involved in DNA replication, DNA repair and cell cycle progression were mostly upregulated. Quantitative PCR experiments validated the array data in all five upregulated (*acta2*, *rrm1*, *pcna*, *mcm4*, *mcm5*) and four downregulated genes (*acta1*, *versicanb*, *mtn1*, *col10a1*) that we tested for both *slc2a10*-MO and LY-364947 treatments (Supplementary Material, Fig. S3).

A relatively large proportion of the genes that showed differential expression in the *slc2a10* knockdown model but not in the LY-364947 treated embryos are involved in the pathways supplying energy to the cell (Supplementary Material, Table S3). Several of these genes belong to the oxidative phosphorylation pathway (*cyc1*, *ndufab1*), the concomitant reactive oxygen production pathway (*sod2*, *gpx4a*, *ant*, *mpx*), the Szent–Györgyi–Krebs cycle (*mdh1b*, *got2a* and *slc13a2*), the glycolysis/gluconeogenesis pathway (*eno2*, *pkm2b*, *tpi1a*, *pfkm*) and glycogen metabolism (*gys2*, *gygl*). In addition, several genes involved in calcium binding and homeostasis and the production of heme or hemoproteins in the mitochondria were uniquely downregulated in the *slc2a10* knockdown model. Also, several components of the contractile muscle cytoskeleton, the connective tissue and the cardiovascular system showed differential expression patterns specifically upon *slc2a10* knockdown. Finally, compared with the LY-364947 treatment, additional genes involved in DNA replication, DNA repair and cell cycle progression were upregulated when *slc2a10* was depleted. We selected 6 upregulated (*mpx*, *pfkm*, *hmbsl*, *tnnt1*, *fn1b*, *mmp13*) and 19 downregulated (*sod2*, *tpi1a*, *ndufab1*, *cyc*, *eno2*, *got2a*, *pkm2b*, *gys2*, *mdh1b*, *slc13a2*, *cyc1*, *gpx4a*, *slc25a4*, *gygl*, *ppox*, *pvalb2*, *pvalb5*, *mybpc3*, *agt*) transcripts to validate *slc2a10* knockdown-specific changes by qPCR and in each case the direction and magnitude of change were replicated (Supplementary Material, Fig. S4).

Slc2a10 is required for mitochondrial function

To test whether altered mitochondrial gene expression caused structural anomalies, we examined mitochondria in *slc2a10*-MO (7.5 ng) and control-MO (5 ng) treated embryos at 52 hpf by transmission electron microscopy. No remarkable morphological change was found in the mitochondria in *slc2a10* knockdown embryos (Fig. 6A and B). To investigate whether glut10-deficient mitochondria were functionally impaired, we measured the oxygen consumption of control- and *slc2a10*-MO-treated embryos using a Seahorse XF24 extracellular flux analyzer. Knockdown of *slc2a10* resulted

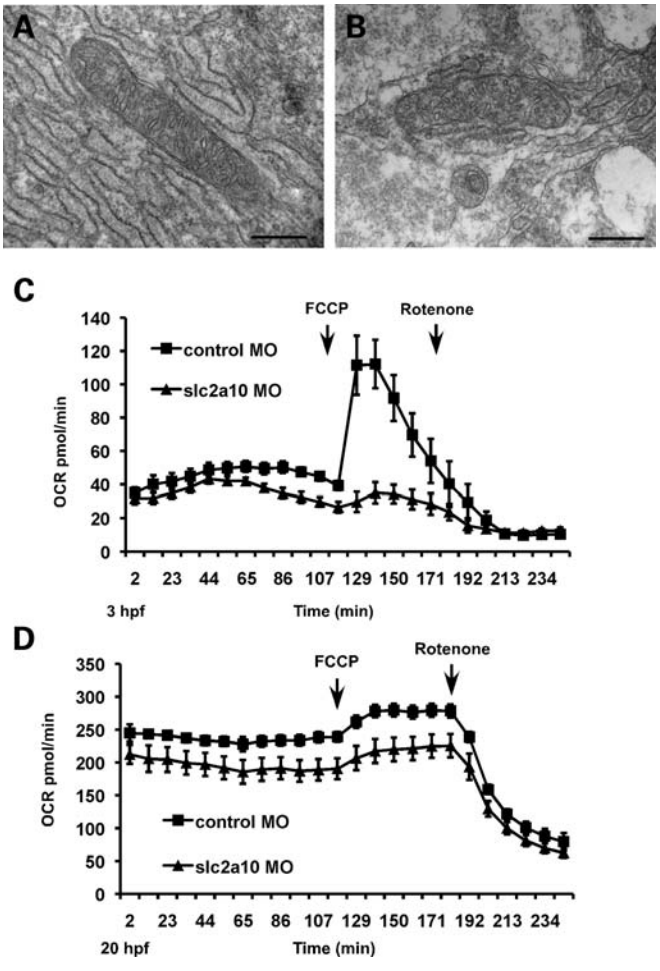

Figure 6. Knockdown of *slc2a10* does not affect mitochondrial morphology but decreases the OCR. Electron micrographs of mitochondria from control-MO-injected (**A**) and *slc2a10*-MO-injected (**B**) embryos at 52 hpf show normal morphology. Magnification bars: 500 nm. The measurement of OCR of control-MO and *slc2a10*-MO-injected embryos at 3–11 hpf (**C**) and at 20–28 hpf (**D**). FCCP, an uncoupler, and rotenone (a complex I inhibitor) were added at the indicated time points.

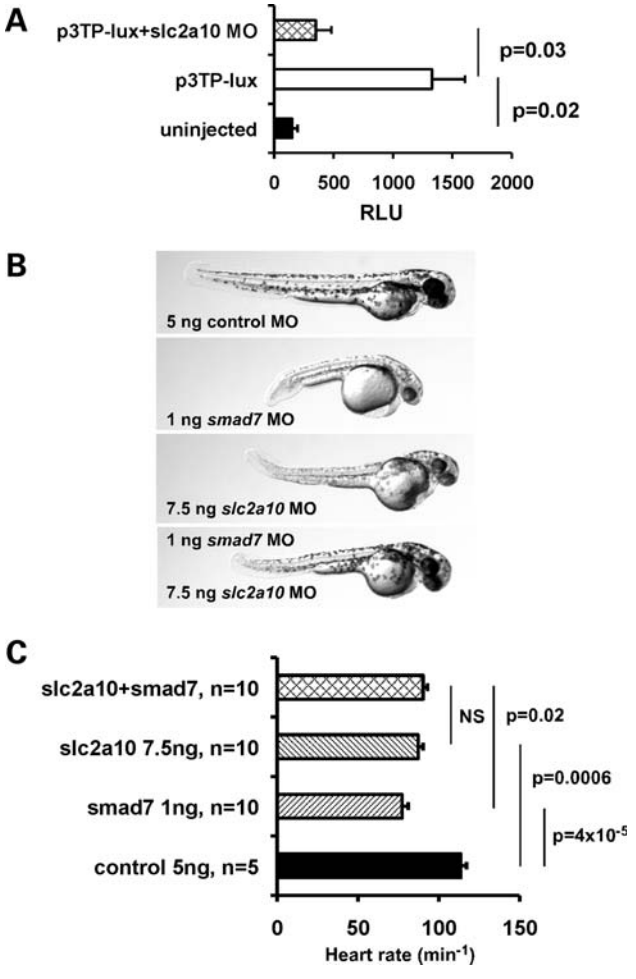

Figure 7. Knockdown of *slc2a10* downregulates TGFβ-like transcriptional responses and rescues smad7 morphant phenotypes. (**A**) A p3TP-lux TGFβ-responsive reporter construct was injected in the presence or in the absence slc2a10-MO. Luciferase activity was assayed at 24 hpf from embryo lysates and compared with uninjected embryos. Pairwise comparison of experimental groups was performed using Student's *t*-test with *P*-values shown on the right. RLU, relative light units. (**B**) Partial rescue of *smad7* morphants by simultaneous administration of *slc2a10*-MO as viewed at 48 hpf. Administration of 1 ng *smad7*-MO causes severely shortened tail, underdeveloped mesodermal tissues, small head and pericardiac edema. Injection of 7.5 ng of *slc2a10*-MO caused milder shortening and bending of the embryo and pericardiac edema. The combination of 1 ng *smad7* and 7.5 ng *slc2a10*-MO showed a marked improvement in the tail length, head size and heart morphology relative to *smad7*-MO treatment only. (**C**) The heart rate of *smad7* morphants was severely reduced compared with control-MO-injected embryos. A smaller decrease was observed in response to *slc2a10*-MO, combined treatment of embryos with *slc2a10*- and *smad7*-MO improved the heart rate relative to *smad7*-MO only.

in a significant, 20–25% reduction in oxygen consumption rate (OCR) starting at 4 hpf (Fig. 6C) and lasting through 24 hpf (Fig. 6D and data not shown).

Chemicals or endogenous proteins can equalize the electrochemical potential gradient between the matrix and the intermembrane space of mitochondria, thus uncoupling ATP synthesis from the electron transport chain (20). Uncoupling in turn releases the 'backpressure' on the proton transporters of the electron transport chain allowing metabolic oxidation to proceed at a maximal rate. To probe the capacity of the electron transport chain, we administered a chemical uncoupler (FCCP, carbonyl cyanide *p*-trifluoromethoxy-phenylhydrazone) to the embryos. FCCP treatment significantly increased the OCR in control embryos causing a 3-fold increase at 5 hp and a smaller, 20% increase at 22 hpf (Fig. 6C and D). In contrast, *slc2a10* morphants showed no increase in respiration in response to FCCP, indicating that both the physiological and the maximal capacity of the electron transport chain were reduced in the absence of glut10. Treatment of embryos with rotenone, an inhibitor of complex I, reduced respiration in both control and *slc2a10* morphant embryos to the same baseline level (Fig. 6C and D), providing further proof of the specificity of our assay for mitochondrial respiration.

Slc2a10 is required for TGFβ signaling

Similarities in phenotypes and gene expression profiles between chemical inhibition of TGFβ signaling and *slc2a10* knockdown provide a large body of correlative evidence supporting a role for *slc2a10* as a facilitator of TGFβ

signaling. To obtain more direct evidence and to begin to map the location of glut10 in the TGFβ pathway, we performed two experiments. First, we injected a TGFβ-responsive luciferase reporter construct (p3TP-lux) into embryos. The promoter in this construct contains three TPA (12-*O*-tetradecanoylphorbol-13-acetate) response elements and a part of the plasminogen activator inhibitor 1 (PAI1) promoter (21), and has previously been shown to be active in zebrafish (22). Simultaneous injection of *slc2a10*-MO resulted in a 75% reduction of promoter activity compared with p3TP-lux only (Fig. 7A).

If the loss of glut10 function indeed results in depressed TGFβ-dependent transcriptional responses, as our results thus far show, we reasoned that glut10 knockdown might rescue the phenotypic effects of artificially elevated TGFβ activity. To create a state of increased TGFβ signaling in embryos, we knocked down smad7, an endogenous inhibitor of tgfbr1 signaling. Moderate concentrations (5 ng) of a *smad7* splice morpholino resulted in a complete arrest of the development of embryos at the mid-blastula transition (3–4 hpf) and death by 8 hpf (data not shown). At lower MO concentrations (1 ng), *smad7* knockdown permitted the development of the embryo through gastrulation and organogenesis but resulted in a recognizable pattern of malformations, including small head and eyes, pericardial edema, severely shortened tail, underdeveloped muscle and notochord (Fig. 7B). Injection of *slc2a10*-MO alone caused the previously described phenotype with bent notochord, shorter embryo and pericardial edema.

Combined injection of *smad7* and *slc2a10*-MO resulted in a phenotype showing a significant improvement over *smad7*-MO alone in length, head size, cardiac morphology and the overall volume of mesodermal derivatives (Fig. 7B). However, the combination treatment did not result in an improvement over *glut10*-MO treatment alone. Heart rate, a quantitative measure of cardiovascular function, showed similar changes, with severe (32%) reduction in response to *smad7*-MO treatment only and a 17% improvement with combined treatment (Fig. 7C). The heart rate of *slc2a10* morphants was reduced by 24% relative to control, but combination treatment with smad7-MO did not improve this further.

DISCUSSION

We present an ATS zebrafish model, generated by MO-based knockdown of the *slc2a10* gene, which encodes the glut10 protein. Two MOs, targeting the *slc2a10* start codon and the exon 2–intron 2 donor splice site, respectively, produced identical phenotypes underscoring the specificity of the MOs for *slc2a10* as the likelihood of both MOs mistargeting the same gene is very small (23). The most prominent features of the morphants were a bowed/wavy appearance of the notochord and tail region and cardiovascular insufficiency. Cardiovascular abnormalities included incomplete and irregular patterning especially of the venous plexus and the intersegmental vessels. The heart rate was significantly reduced and blood pooling frequently observed in the heart and tail regions. These circulatory abnormalities may represent developmental precursors to lesions observed in human ATS: tortuosity and aneurysms of the large blood vessels.

In morphant fish, the notochord appeared bowed, kinked and shortened. The notochord consists of large mesodermal cells, packed within a sheath of connective tissue. It represents a primitive form of cartilage that defines the primitive longitudinal skeletal axis of the embryo that guides the formation of the vertebral column. It also provides key signals to the development of other mesodermal derivatives, including the vasculature (24). Therefore, it is unclear whether the notochord abnormalities contribute to the vascular patterning defects that we observed following *slc2a10* knockdown. It has been shown that early curvature of the notochord in zebrafish embryos can result in a scoliotic adult phenotype (25). Similar to our zebrafish model, vertebral column abnormalities, including scoliosis, have been observed in human ATS (5).

Previously, it has been shown that TGFβ signaling is upregulated in vascular smooth muscle cells of ATS patients (6). This might, at least in part, be responsible for the phenotypic abnormalities encountered in ATS patients, especially because a link between elevated TGFβ signaling and connective tissue defects has been shown in related syndromes, including the Marfan, Loeys–Dietz and some cutis laxa syndromes (8,10,12,26). Surprisingly, we found downregulation, rather than upregulation, of total-body TGFβ signaling in *slc2a10* knockdown zebrafish embryos based on five lines of evidence. First, treatment of wild-type embryos with a tgfbr1 inhibitor resulted in a phenotype similar to the ATS zebrafish model, with a bowed notochord/tail region and comparable cardiovascular abnormalities. Secondly, treatment of *scl2a10* morphants with tgfbr1 inhibitor aggravated the phenotype. Thirdly, transcriptional profiling showed a significant correlation between the mRNA profile of *slc2a10* knockdown and tgfbr1 inhibition. The genes affected by both treatments are related to the development of the cardiovascular system, the eye, neurogenesis and cartilage formation. Involvement of TGFβ signaling in these functions has been demonstrated before (2,27–29). Fourthly, the TGFβ reporter construct 3TP-lux showed reduced promoter activity in response to *slc2a10* knockdown. Fifthly, *slc2a10* knockdown partially rescued the deleterious effects of reduced levels of smad7, but not *vice versa*. This suggests that glut10 exerts its effect on TGFβ signaling downstream of smads.

It is possible that TGFβ downregulation during early embryogenesis causes a compensatory upregulation later in development. Such a mechanism has been shown in a *Tgfbr1* (*Alk5*) knockout mouse model. A compensatory upregulation of the ALK5 downstream pathway was noted in these mice to be mediated by activin/ALK4 signaling (30). Also, reduced TGFβ signaling caused by initially elevated sequestration may be followed by an excessive TGFβ release from a defective ECM later in life. Impaired elastic fiber formation, an important feature of ATS patients (31), results in a higher amount of 'bare' microfibrils that can sequester TGFβ in the ECM. As TGFβ activation is dependent on mechanical forces (32), TGFβ release may increase severely once sufficient intravascular pressure exists, a physiological variable that increases through development.

Our expression study also provides new insights into the specific molecular mechanisms involved in the ATS phenotype, as some pathways are altered by *slc2a10* knockdown but not by tgfbr1 inhibition. A key finding is the

downregulation of major players in cellular respiration, a process that converts glucose to the high-energy compound ATP through sequential steps of glycolysis in the cytoplasm, the Szent–Györgyi–Krebs cycle, and the oxidative phosphorylation in the mitochondria. In addition, specifically affected genes in the *slc2a10* knockdown model involve the reactive oxygen species production pathway, heme biosynthesis and Ca^{2+} homeostasis, all important mitochondrial functions. Thus, the differential expression pattern overall points to a contribution of mitochondrial dysfunction in the phenotype caused by the loss of glut10 function in the zebrafish embryo.

Mitochondrial dysfunction in *slc2a10* knockdown embryos was confirmed by our extracellular flux measurements. In spite of relatively preserved mitochondrial morphology, the loss of glut10 caused reduced overall respiration and reduced maximal flux of the electron transport chain in response to uncoupler administration. Reduced electron transport chain activity in *slc2a10* knockdown embryos is consistent with reduced gene expression of electron transport chain components NADH-ubiquinone oxidoreductase 1 alpha/beta subcomplex (ndufab1) and cytochrome C1 (cyc1) (Supplementary Material, Table S2).

Mitochondrial dysfunction observed through altered transcriptional profiles in our study is consistent with the recent finding that GLUT10 is required for dehydroascorbic acid (DHA) transport into the mitochondria (33). DHA is converted to the antioxidant ascorbic acid that reduces reactive oxygen species generated as a result of oxidative phosphorylation. Consequently, defective recycling of DHA in the absence of GLUT10 results in increased sensitivity of cells to oxidative damage (33), which is expected to lead to alterations in the expression of genes required for mitochondrial function as observed in our study.

GLUT10 deficiency results in severe cardiovascular and connective tissue manifestations in both humans (5,6) and zebrafish (this study). In contrast, inactivating mutations in mouse Glut10 result in a mild, subclinical phenotype (13,14). Differences in vitamin C metabolism among species may explain these observations. Some vertebrates, including humans and teleost fish but not mice, lack gulonolactone oxidase, a key enzyme in the biosynthetic pathway of vitamin C (34). These organisms depend on dietary vitamin C and efficient intracellular recycling of this antioxidant and thus may be more susceptible to the loss of GLUT10, a DHA transporter.

Because a primary mitochondrial abnormality in our study led to decreased expression of TGFβ target genes, we conclude that at least a part of the TGFβ signaling pathway is dependent on mitochondrial function. Consistent with this notion, several studies highlighted connections between mitochondria, oxidative stress and TGFβ signaling (35–38). This may occur through the coupling of intracellular oxidative pathways and TGFβ signaling by the renin–angiotensin pathway. Indeed, the angiotensinogen transcript is downregulated in the *slc2a10* knockdown model and this molecule is known to enhance TGFβ signaling and ECM metabolism (39,40).

Mitochondrial dysfunction in relation to oxidative stress has recently been shown to be involved in the pathogenesis of other connective tissue disorders related to ATS. Mutations in the *PYCR1* gene encoding Δ-1-pyrroline-5-carboxylate reductase 1, an mitochondrial enzyme involved in proline metabolism, cause autosomal-recessive cutis laxa type IIB, wrinkly skin syndrome and geroderma osteodysplasticum (41). Together with our findings, this illustrates that proper mitochondrial function is essential for the development and maintenance of connective tissues, in part through interactions with the TGFβ signaling pathway.

MATERIALS AND METHODS

Zebrafish maintenance and microscopy

Wild-type AB and transgenic *Tg(Fli1:EGFP)*^{y1} zebrafish were reared at a constant temperature of 25°C and maintained on a 14-h light, 10-h dark photoperiod. Fish were fed three times daily with both micropellets (Hikari, Hayward, CA, USA) and brine shrimp (Biomarine, Aquafauna Bio-Marine, Hawthorne, CA, USA). After *in vitro* fertilization, dead embryos were removed at 8 hpf and surviving embryos were treated with 1-phenyl-2-thiourea to inhibit melanin pigmentation, dechorionated with pronase (Sigma, St. Louis, MO, USA) at 24 hpf and examined at 48 hpf. Microinjection procedures were performed using an Olympus SZX7 stereomicroscope. Live embryos were mounted in 2% methylcellulose and imaged using an Olympus MVX 10 (bright field and fluorescent) microscope equipped with Olympus MicroSuite software. For confocal microscopy, live embryos were anesthetized with tricaine, mounted in 1% low-melting agarose and imaged using a laser-scanning Olympus FV500 confocal microscope utilizing a ×10 objective. Statistical analysis was conducted using a non-parametric Kruskal–Wallis test followed by Dunn's multiple comparison post hoc test or χ^2 followed by Bonferroni correction.

Morpholino-mediated knockdown

Antisense MOs (Genetools, Philomath, OR, USA) such as ATG-MO (5′-TCAGGAGCAGGACAGAACAACCCAT-3′) and splice-MO (5′-CAAATAAAGTCCACTTACTTGGT CC-3′) were directed against exons 1 and 2 regions spanning the *slc2a10* ATG start codon and the exon 2–intron 2 donor splice site of the *slc2a10* pre-mRNA, respectively. The MO against *smad7* (5′-ATGAAACTTCAACTTACCAGGTG GT-3′) was also directed against the exon 2–intron 2 donor splice site. A standard control-MO (5′-CCTCTTACCTC AGTTACAATTTATA-3′) was used as a control. Routinely, MOs were microinjected in 1–5 nl volume into 1- to 2-cell stage embryos at 2.5 ng for *slc2a10* ATG-MO, 7.5 ng for *slc2a10* splice-MO and 5 ng for control-MO and 1 ng for *smad7*-MO. All MOs were dissolved in 0.2% phenol red and 1× Danieu's buffer [58 mM NaCl, 0.7 mM KCl, 0.4 mM $MgSO_4$, 0.6 mM $Ca(NO_3)_2$, 5.0 mM HEPES (pH 7.6)].

Real-time qPCR

After homogenization of ten to fifteen 48 hpf zebrafish embryos, total RNA was isolated with TRIzol reagent (Invitrogen) and cDNA synthesis was performed using the SuperScript III First-Strand Synthesis System for RT–PCR with random hexamer

primers (Invitrogen) in a total volume of 20 μl. Amplification efficiency (E) for each primer set was determined on the basis of a 6-fold zebrafish cDNA dilution series. Only primer pairs with $E \geq 85\%$ were used for further experiments. PCR mixtures contained ABI SYBR Green PCR Master Mix, 0.25 μM of each forward and reverse primer and 10 ng cDNA. Cycling conditions were as follows: 10 min at 95°C, 40 cycles at 95°C for 15s, 60°C for 60 s. Subsequently, a melting curve (55–95°C) was generated for every amplicon to check PCR specificities. qPCR analysis was performed on Stratagene Mx3005P qPCR system (Agilent Technologies, Santa Clara, CA, USA). All reactions were carried out in triplicate and normalized to the geometric mean of two stable reference genes, *bactin I* and *elfa*, using qBasePlus software (42,43). Expression levels were determined in three independent experiments for each RNA extraction. Differential gene expression was considered significant if the means differed by at least 50 and the 95% confidence intervals of the means did not overlap (equivalent to $P < 0.05$). Oligonucleotide primers used for qPCR are available upon request.

Pharmacologic treatment

Transforming growth factor-β type I receptor kinase inhibitor or ALK5 inhibitor I [3-(pyridin-2-yl)-4-(4-quinonyl)]-1H-pyrazole] (LY-364947 or HTS-466284, #616451, EMD Chemicals, Gibbstown, NJ, USA) was prepared as a 20 mM stock in dimethyl sulfoxide. Working solutions were made in E3 chemical screening medium (44). Embryos were incubated in the compound starting at 8 hpf, dechorionated at 24 hpf and examined at 48 hpf.

Array hybridization

After quantification and quality control, RNA samples were subjected to T7 linear amplification. Amplified RNAs were chemically labeled with either cy3 or cy5 dyes. Labeled RNA samples were quantified, equalized by mass, paired and combined to test treatment effects. Three biological replicates were used. The paired and balanced RNAs were suspended in Agilent 2× Gene Expression buffer (55 μl), Agilent 10× Blocking agent (11 μl) and Kreablock (27.5 μl). The hybridization solutions were applied to Agilent Zebrafish v2 4 × 44K microarrays. Hybridization was carried out at 65°C for 20 h. Washing procedures were carried out according to Agilent gene expression protocols. Slides were scanned on an Axon 4000B scanner to detect Cy3 and Cy5 fluorescence. Laser power was kept constant for Cy3/Cy5 scans and the photomultiplier tube setting (PMT) was varied for each experiment based on the optimal signal intensity with lowest possible background fluorescence. A low PMT setting scan was also performed to recover signals from saturated elements. Gridding and analysis of images was performed using Genepix v6.1 (Axon, Molecular Devices, Sunnyvale, CA, USA). A Partek Genomics Suite (Partek, St. Louis, MO, USA) was used to normalize and statistically analyze the data. The microarray data set has been deposited into the NCBI Gene Expression Omnibus (http://www.ncbi.nlm.nih.gov/geo/) and is available through accession number GSE34510.

Electron microscopy

Embryos were dechorionated at 52 hpf, fixed in glutaraldehyde, stained sequentially with OsO_4, tannic acid and uranyl acetate, dehydrated and embedded in Epon (45). Thin sections (60 nm) were cut, placed on formvar-coated grids and counterstained with 7% methanolic uranyl acetate and lead citrate. Sections were viewed with a Tecnai 12 transmission electron microscope at 120 kV, and the images were digitally captured.

The OCR measurement

The OCR was measured in developing zebrafish embryos using XF24 Extracellular Flux Analyzer (Seahorse Bioscience, Billerica, MA, USA). Four control or *slca2a10*-MO-injected embryos were loaded into each of 5–10 wells of XF24 islet capture microplates (Seahorse Bioscience) at 3 or 20 hpf and incubated at 37°C in E3 solution. After an OCR measurement of 2 h, FCCP was added to 1 μM final concentration and incubated for 1 h. Next, rotenone was added to each well to reach a final concentration of 4 μM followed by a 1 h incubation. The OCR measurements were taken every 6 min after a 3 min mixing period.

Luciferase assay

To verify the role of glut10 in facilitating TGFβ signaling, 1-cell stage wild-type embryos were co-injected with 75 pg pgl2-basic 3TP-lux with 7.5 ng *slc2a10*-MO or 5 ng control-MO. Ten embryos per replicate were harvested at 24 hpf and lysed in reporter lysis buffer (Promega, Madison, WI, USA) using a pestle homogenizer. The lysates were cleared by centrifugation at 13 000 rpm in a microcentrifuge, and a 10-μl aliquot of each of the four biological replicates were analyzed using a luciferase assay system (Promega) and a Genios plate reader (Tecan, Durham, NC, USA) and results were recorded in relative luminescence units (RLUs). An aliquot of the lysates was used to measure the protein concentration. As all protein concentrations were within ±10% of the mean, we did not correct the RLU readings for protein concentration.

SUPPLEMENTARY MATERIAL

Supplementary Material is available at *HMG* online.

ACKNOWLEDGEMENTS

We thank Dr Mary O. Carayannopoulos for advice on the glut family of proteins, Dr Matthew I. Goldsmith for help with zebrafish methods, Michael E. Heinz for technical help with array hybridization and Dr Beth L. Roman for the p3TP-lux plasmid. We appreciate the support of the Washington University Pediatric Zebrafish Facility and the University of Pittsburgh Zebrafish Facility.

Conflict of Interest statement: None declared.

FUNDING

This work was supported by the National Institutes of Health (HL084922, HL090648 to Z.U.), by the March of Dimes (#1-FY09-402 to Z.U.), by Ghent University (Methusalem grant BOF08/01M01108 to A.D.P.) and by the Fighting Aneurysmal Disease (EC-FP7 to P.J.C. and A.D.P.). A.W. was a research fellow and B.L.C is a postdoctoral fellow of the Fund for Scientific Research – Flanders. The Genome Technology Access Center in the Department of Genetics at Washington University School of Medicine assisted with genomic analysis. The center is partially supported by NCI Cancer Center Support Grant #P30 CA91842 to the Siteman Cancer Center and by ICTS/CTSA Grant# UL1RR024992 from the National Center for Research Resources (NCRR), a component of the National Institutes of Health (NIH), and NIH Roadmap for Medical Research. This publication is solely the responsibility of the authors and does not necessarily represent the official view of NCRR or NIH.

REFERENCES

1. Ma, X.M. and Blenis, J. (2009) Molecular mechanisms of mTOR-mediated translational control. *Nat. Rev. Mol. Cell Biol.*, **10**, 307–318.
2. Goumans, M.J., Liu, Z. and ten Dijke, P. (2009) TGF-beta signaling in vascular biology and dysfunction. *Cell Res.*, **19**, 116–127.
3. Nian, M., Lee, P., Khaper, N. and Liu, P. (2004) Inflammatory cytokines and postmyocardial infarction remodeling. *Circ. Res.*, **94**, 1543–1553.
4. Hayden, M.R. and Reidy, M. (1995) Many roads lead to atheroma. *Nat. Med.*, **1**, 22–23.
5. Callewaert, B.L., Willaert, A., Kerstjens-Frederikse, W.S., De Backer, J., Devriendt, K., Albrecht, B., Ramos-Arroyo, M.A., Doco-Fenzy, M., Hennekam, R.C., Pyeritz, R.E. *et al.* (2008) Arterial tortuosity syndrome: clinical and molecular findings in 12 newly identified families. *Hum. Mutat.*, **29**, 150–158.
6. Coucke, P.J., Willaert, A., Wessels, M.W., Callewaert, B., Zoppi, N., De Backer, J., Fox, J.E., Mancini, G.M., Kambouris, M., Gardella, R. *et al.* (2006) Mutations in the facilitative glucose transporter GLUT10 alter angiogenesis and cause arterial tortuosity syndrome. *Nat. Genet.*, **38**, 452–457.
7. Neptune, E.R., Frischmeyer, P.A., Arking, D.E., Myers, L., Bunton, T.E., Gayraud, B., Ramirez, F., Sakai, L.Y. and Dietz, H.C. (2003) Dysregulation of TGF-beta activation contributes to pathogenesis in Marfan syndrome. *Nat. Genet.*, **33**, 407–411.
8. Loeys, B.L., Chen, J., Neptune, E.R., Judge, D.P., Podowski, M., Holm, T., Meyers, J., Leitch, C.C., Katsanis, N., Sharifi, N. *et al.* (2005) A syndrome of altered cardiovascular, craniofacial, neurocognitive and skeletal development caused by mutations in TGFBR1 or TGFBR2. *Nat. Genet.*, **37**, 275–281.
9. Hucthagowder, V., Sausgruber, N., Kim, K.H., Angle, B., Marmorstein, L.Y. and Urban, Z. (2006) Fibulin-4: a novel gene for an autosomal recessive cutis laxa syndrome. *Am. J. Hum. Genet.*, **78**, 1075–1080.
10. Renard, M., Holm, T., Veith, R., Callewaert, B.L., Ades, L.C., Baspinar, O., Pickart, A., Dasouki, M., Hoyer, J., Rauch, A. *et al.* (2010) Altered TGFbeta signaling and cardiovascular manifestations in patients with autosomal recessive cutis laxa type I caused by fibulin-4 deficiency. *Eur. J. Hum. Genet.*, **18**, 895–901.
11. Cohn, R.D., van Erp, C., Habashi, J.P., Soleimani, A.A., Klein, E.C., Lisi, M.T., Gamradt, M., ap Rhys, C.M., Holm, T.M., Loeys, B.L. *et al.* (2007) Angiotensin II type 1 receptor blockade attenuates TGF-beta-induced failure of muscle regeneration in multiple myopathic states. *Nat. Med.*, **13**, 204–210.
12. Habashi, J.P., Judge, D.P., Holm, T.M., Cohn, R.D., Loeys, B.L., Cooper, T.K., Myers, L., Klein, E.C., Liu, G., Calvi, C. *et al.* (2006) Losartan, an AT1 antagonist, prevents aortic aneurysm in a mouse model of Marfan syndrome. *Science*, **312**, 117–121.
13. Callewaert, B.L., Loeys, B.L., Casteleyn, C., Willaert, A., Dewint, P., De Backer, J., Sedlmeier, R., Simoens, P., De Paepe, A.M. and Coucke, P.J. (2008) Absence of arterial phenotype in mice with homozygous slc2A10 missense substitutions. *Genesis*, **46**, 385–389.
14. Cheng, C.H., Kikuchi, T., Chen, Y.H., Sabbagha, N.G., Lee, Y.C., Pan, H.J., Chang, C. and Chen, Y.T. (2009) Mutations in the SLC2A10 gene cause arterial abnormalities in mice. *Cardiovasc. Res.*, **81**, 381–388.
15. Chico, T.J., Ingham, P.W. and Crossman, D.C. (2008) Modeling cardiovascular disease in the zebrafish. *Trends Cardiovasc. Med.*, **18**, 150–155.
16. Chiarelli, N., Ritelli, M., Zoppi, N., Benini, A., Borsani, G., Barlati, S. and Colombi, M. (2011) Characterization and expression pattern analysis of the facilitative glucose transporter 10 gene (slc2a10) in Danio rerio. *Int. J. Dev. Biol.*, **55**, 229–236.
17. Thisse, C. and Zon, L.I. (2002) Organogenesis—heart and blood formation from the zebrafish point of view. *Science*, **295**, 457–462.
18. Li, H.Y., Wang, Y., Heap, C.R., King, C.H., Mundla, S.R., Voss, M., Clawson, D.K., Yan, L., Campbell, R.M., Anderson, B.D. *et al.* (2006) Dihydropyrrolopyrazole transforming growth factor-beta type I receptor kinase domain inhibitors: a novel benzimidazole series with selectivity versus transforming growth factor-beta type II receptor kinase and mixed lineage kinase-7. *J. Med. Chem.*, **49**, 2138–2142.
19. Singh, J., Chuaqui, C.E., Boriack-Sjodin, P.A., Lee, W.C., Pontz, T., Corbley, M.J., Cheung, H.K., Arduini, R.M., Mead, J.N., Newman, M.N. *et al.* (2003) Successful shape-based virtual screening: the discovery of a potent inhibitor of the type I TGFbeta receptor kinase (TbetaRI). *Bioorg. Med. Chem. Lett.*, **13**, 4355–4359.
20. Lowell, B.B. and Spiegelman, B.M. (2000) Towards a molecular understanding of adaptive thermogenesis. *Nature*, **404**, 652–660.
21. Wrana, J.L., Attisano, L., Carcamo, J., Zentella, A., Doody, J., Laiho, M., Wang, X.F. and Massague, J. (1992) TGF beta signals through a heteromeric protein kinase receptor complex. *Cell*, **71**, 1003–1014.
22. Park, S.O., Lee, Y.J., Seki, T., Hong, K.H., Fliess, N., Jiang, Z., Park, A., Wu, X., Kaartinen, V., Roman, B.L. *et al.* (2008) ALK5- and TGFBR2-independent role of ALK1 in the pathogenesis of hereditary hemorrhagic telangiectasia type 2. *Blood*, **111**, 633–642.
23. Sumanas, S. and Larson, J.D. (2002) Morpholino phosphorodiamidate oligonucleotides in zebrafish: a recipe for functional genomics? *Brief Funct. Genomic Proteomic.*, **1**, 239–256.
24. Fouquet, B., Weinstein, B.M., Serluca, F.C. and Fishman, M.C. (1997) Vessel patterning in the embryo of the zebrafish: guidance by notochord. *Dev. Biol.*, **183**, 37–48.
25. Christiansen, H.E., Lang, M.R., Pace, J.M. and Parichy, D.M. (2009) Critical early roles for col27a1a and col27a1b in zebrafish notochord morphogenesis, vertebral mineralization and post-embryonic axial growth. *PLoS One*, **4**, e8481.
26. Hu, Q., Shifren, A., Sens, C., Choi, J., Szabo, Z., Starcher, B.C., Knutsen, R.H., Shipley, J.M., Davis, E.C., Mecham, R.P. *et al.* (2010) Mechanisms of emphysema in autosomal dominant cutis laxa. *Matrix Biol.*, **29**, 621–628.
27. Gomes, F.C., Sousa Vde, O. and Romao, L. (2005) Emerging roles for TGF-beta1 in nervous system development. *Int. J. Dev. Neurosci.*, **23**, 413–424.
28. Lin, Z., Willers, C., Xu, J. and Zheng, M.H. (2006) The chondrocyte: biology and clinical application. *Tissue Eng.*, **12**, 1971–1984.
29. Saika, S. (2006) TGFbeta pathobiology in the eye. *Lab Invest*, **86**, 106–115.
30. Carvalho, R.L., Itoh, F., Goumans, M.J., Lebrin, F., Kato, M., Takahashi, S., Ema, M., Itoh, S., van Rooijen, M., Bertolino, P. *et al.* (2007) Compensatory signalling induced in the yolk sac vasculature by deletion of TGFbeta receptors in mice. *J. Cell Sci.*, **120**, 4269–4277.
31. Pletcher, B.A., Fox, J.E., Boxer, R.A., Singh, S., Blumenthal, D., Cohen, T., Brunson, S., Tafreshi, P. and Kahn, E. (1996) Four sibs with arterial tortuosity: description and review of the literature. *Am. J. Med. Genet.*, **66**, 121–128.
32. Wipff, P.J., Rifkin, D.B., Meister, J.J. and Hinz, B. (2007) Myofibroblast contraction activates latent TGF-beta1 from the extracellular matrix. *J. Cell Biol.*, **179**, 1311–1323.
33. Lee, Y.C., Huang, H.Y., Chang, C.J., Cheng, C.H. and Chen, Y.T. (2010) Mitochondrial GLUT10 facilitates dehydroascorbic acid import and protects cells against oxidative stress: mechanistic insight into arterial tortuosity syndrome. *Hum. Mol. Genet.*, **19**, 3721–3733.

34. Dabrowski, K. (1990) Gulonolactone oxidase is missing in teleost fish. The direct spectrophotometric assay. *Biol. Chem. Hoppe Seyler*, **371**, 207–214.
35. de Cavanagh, E.M., Ferder, M., Inserra, F. and Ferder, L. (2009) Angiotensin II, mitochondria, cytoskeletal, and extracellular matrix connections: an integrating viewpoint. *Am. J. Physiol. Heart Circ. Physiol.*, **296**, H550–H558.
36. Guo, P., Nishiyama, A., Rahman, M., Nagai, Y., Noma, T., Namba, T., Ishizawa, M., Murakami, K., Miyatake, A., Kimura, S. *et al.* (2006) Contribution of reactive oxygen species to the pathogenesis of left ventricular failure in Dahl salt-sensitive hypertensive rats: effects of angiotensin II blockade. *J. Hypertens.*, **24**, 1097–1104.
37. Mitchell, C., Robin, M.A., Mayeuf, A., Mahrouf-Yorgov, M., Mansouri, A., Hamard, M., Couton, D., Fromenty, B. and Gilgenkrantz, H. (2009) Protection against hepatocyte mitochondrial dysfunction delays fibrosis progression in mice. *Am. J. Pathol.*, **175**, 1929–1937.
38. Zhao, W., Zhao, T., Chen, Y., Ahokas, R.A. and Sun, Y. (2008) Oxidative stress mediates cardiac fibrosis by enhancing transforming growth factor-beta1 in hypertensive rats. *Mol. Cell Biochem.*, **317**, 43–50.
39. Campbell, S.E. and Katwa, L.C. (1997) Angiotensin II stimulated expression of transforming growth factor-beta1 in cardiac fibroblasts and myofibroblasts. *J. Mol. Cell Cardiol.*, **29**, 1947–1958.
40. Schultz Jel, J., Witt, S.A., Glascock, B.J., Nieman, M.L., Reiser, P.J., Nix, S.L., Kimball, T.R. and Doetschman, T. (2002) TGF-beta1 mediates the hypertrophic cardiomyocyte growth induced by angiotensin II. *J. Clin. Invest.*, **109**, 787–796.
41. Reversade, B., Escande-Beillard, N., Dimopoulou, A., Fischer, B., Chng, S.C., Li, Y., Shboul, M., Tham, P.Y., Kayserili, H., Al-Gazali, L. *et al.* (2009) Mutations in PYCR1 cause cutis laxa with progeroid features. *Nat. Genet.*, **41**, 1016–1021.
42. Hellemans, J., Mortier, G., De Paepe, A., Speleman, F. and Vandesompele, J. (2007) qBase relative quantification framework and software for management and automated analysis of real-time quantitative PCR data. *Genome Biol.*, **8**, R19.
43. McCurley, A.T. and Callard, G.V. (2008) Characterization of housekeeping genes in zebrafish: male–female differences and effects of tissue type, developmental stage and chemical treatment. *BMC Mol. Biol.*, **9**, 102.
44. Murphey, R.D. and Zon, L.I. (2006) Small molecule screening in the zebrafish. *Methods*, **39**, 255–261.
45. Davis, E.C. (1993) Smooth muscle cell to elastic lamina connections in developing mouse aorta. Role in aortic medial organization. *Lab. Invest.*, **68**, 89–99.
46. Larkin, M.A., Blackshields, G., Brown, N.P., Chenna, R., McGettigan, P.A., McWilliam, H., Valentin, F., Wallace, I.M., Wilm, A., Lopez, R. *et al.* (2007) Clustal W and Clustal X version 2.0. *Bioinformatics*, **23**, 2947–2948.
47. Dawson, P.A., Mychaleckyj, J.C., Fossey, S.C., Mihic, S.J., Craddock, A.L. and Bowden, D.W. (2001) Sequence and functional analysis of GLUT10: a glucose transporter in the Type 2 diabetes-linked region of chromosome 20q12–13.1. *Mol. Genet. Metab.*, **74**, 186–199.
48. Joost, H.G. and Thorens, B. (2001) The extended GLUT-family of sugar/polyol transport facilitators: nomenclature, sequence characteristics, and potential function of its novel members (review). *Mol. Membr Biol.*, **18**, 247–256.